Supplementary Information

Rational design carbon electrode of thermoelectrochemical cells for efficient low-grade heat harvest

Xinyan Zhuang[a], Hongrun Jin[a], Boyang Yu[a], Hui Wang[a], Yongxin Luo[a], Kaisi Liu[a], Bin Hu[a], Kefeng Xie[b,*], Liang Huang[a, *], Jiangjiang Duan[a, *] and Jun Zhou[a]

[a] Wuhan National Laboratory for Optoelectronics, School of Optical and Electronic Information, Huazhong University of Science and Technology, Wuhan, 430074, China.

[b] School of Chemical and Biological Engineering, Lanzhou Jiaotong University, Lanzhou, 730000, China

*Corresponding authors' e-mail addresses:
jiangjduan@hust.edu.cn; huangliang421@hust.edu.cn; xiekefeng@mail.lzjtu.cn

Supplementary Figures

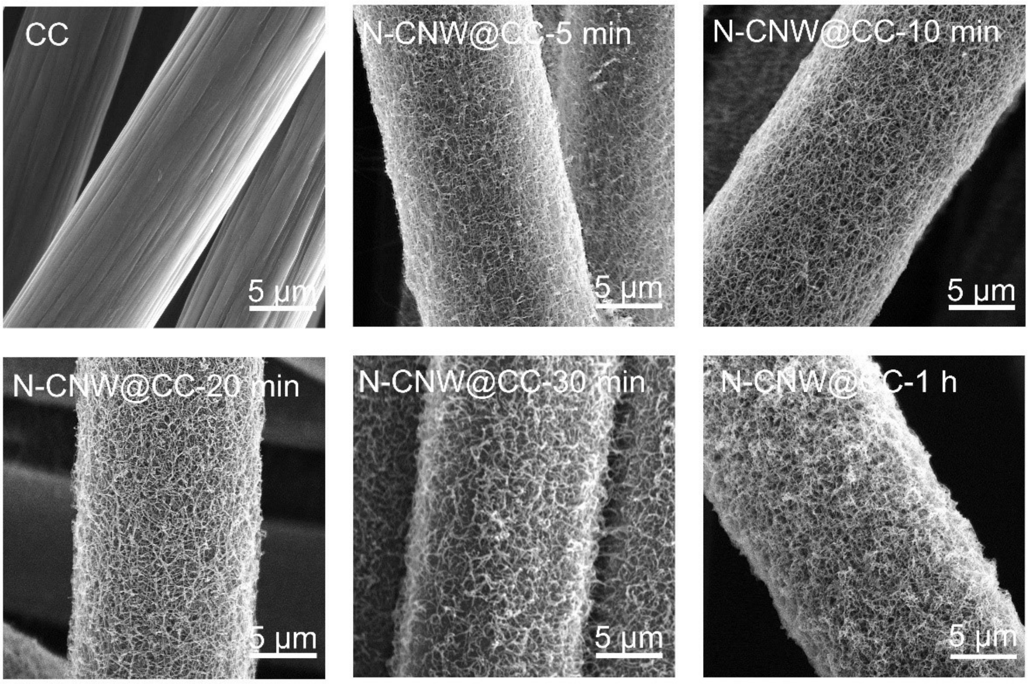

Fig. S1. SEM images of N-CNW@CC with different electrochemical polymerization times.

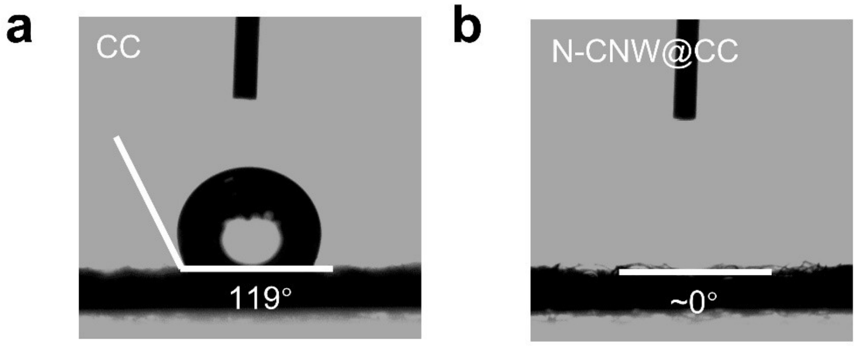

Fig. S2. The contact angle of original (a) carbon cloth and (b) N-CNW@CC.

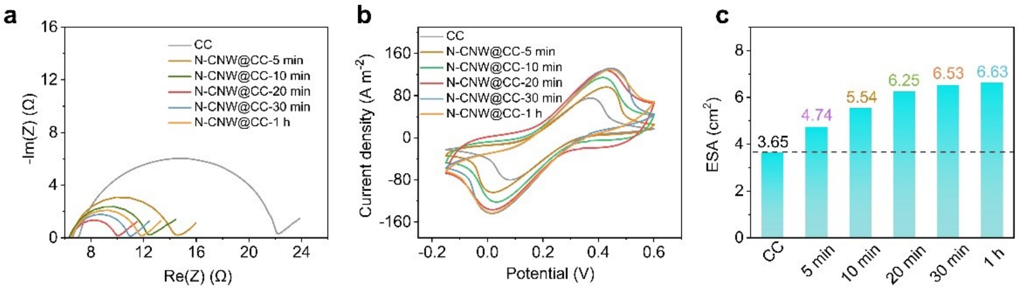

Fig. S3. The effects of electrochemical polymerization time. (a)Nyquist impedance plots (10kHz~50mHz), (b) Cyclic voltammograms (100mV s^{-1}) and (c) Electroactive surface area (ESA) calculated by Randles-Sevcik equation for N-CNW@CC with different electrochemical polymerization time.

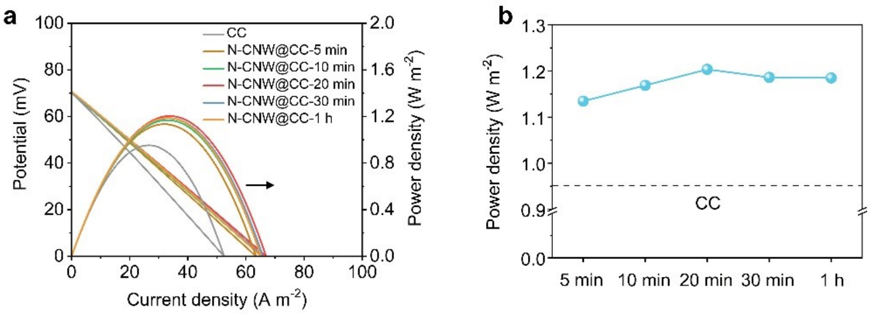

Fig. S4. (a) Current-voltage curves and their corresponding power densities for samples with different electrochemical polymerization times. (ΔT=50°C). (b) The changing trend of $P_{\max}$ with increasing electrochemical polymerization time.

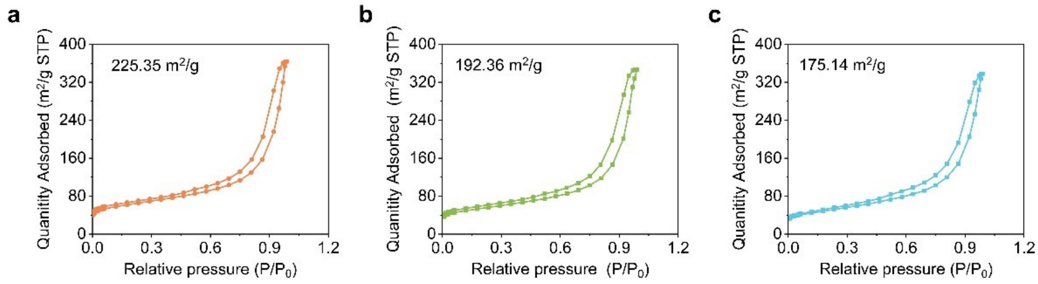

Fig. S5. N_2 sorption isotherm curves of the N-CNW@CC annealed at (a) 700^{o}C, (b) 800^{o}C, (c) 900^{o}C.

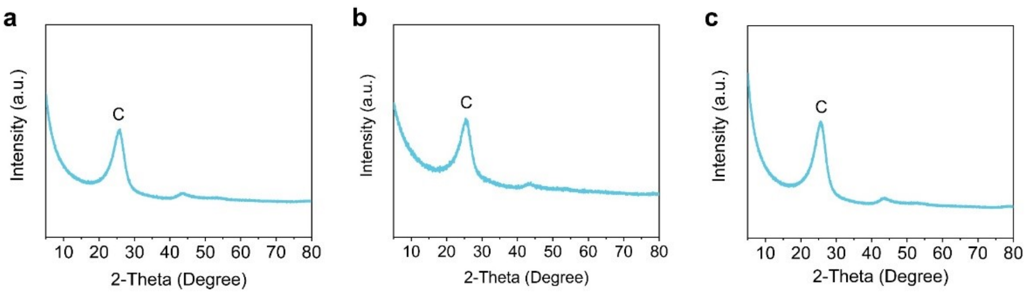

Fig. S6. XPS spectra of the N-CNW@CC annealed at (a) 700^{o}C, (b) 800^{o}C, (c) 900^{o}C.

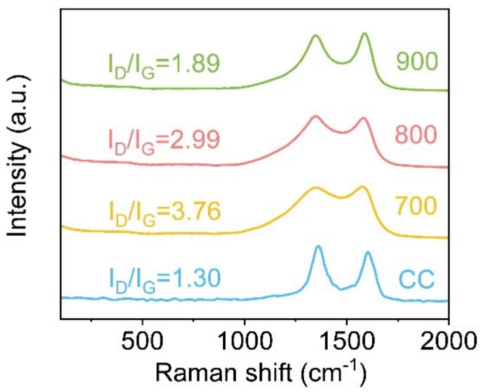

Fig. S7. Raman spectroscopy of electrodes annealed at 700, 800, 900^{o}C.

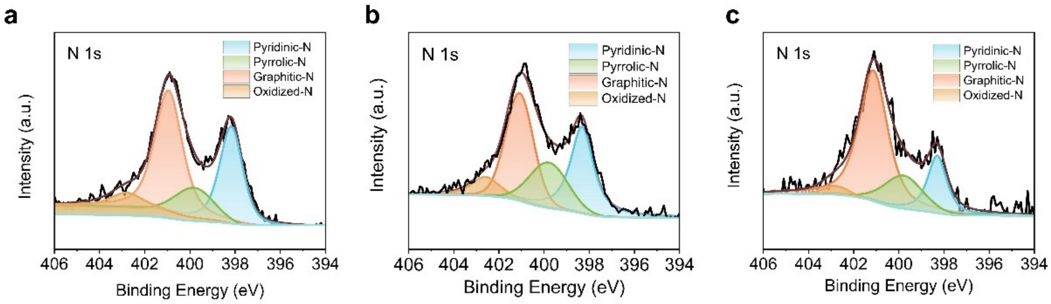

Fig. S8. N 1s XPS spectra of the N-CNW@CC annealed at (a) 700^{o}C, (b) 800^{o}C, (c) 900^{o}C.

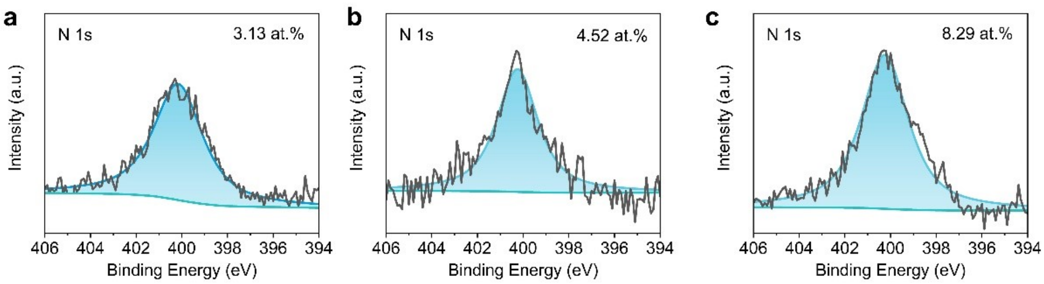

Fig. S9. N1s XPS spectra of single pyrrolic-nitrogen-doped carbon with nitrogen and carbon source mass ratios of (a) 1:7, (b) 1:3 and (c) 1:1.

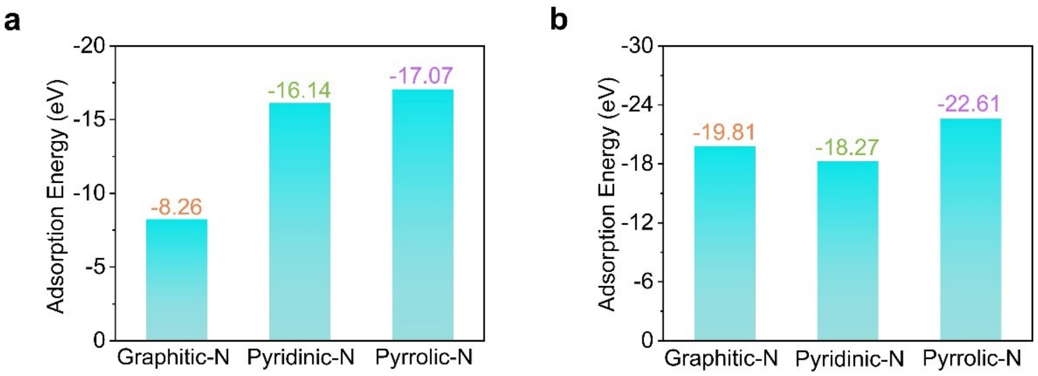

Fig. S10. Simulation calculation of adsorption energy of $Fe(CN)_6^{3-}$ and $Fe(CN)_6^{4-}$. Adsorption energies of (a) $Fe(CN)_6^{3-}$ and (b) $Fe(CN)_6^{4-}$ on pyrrolic-N, pyridinic-N, graphitic-N.

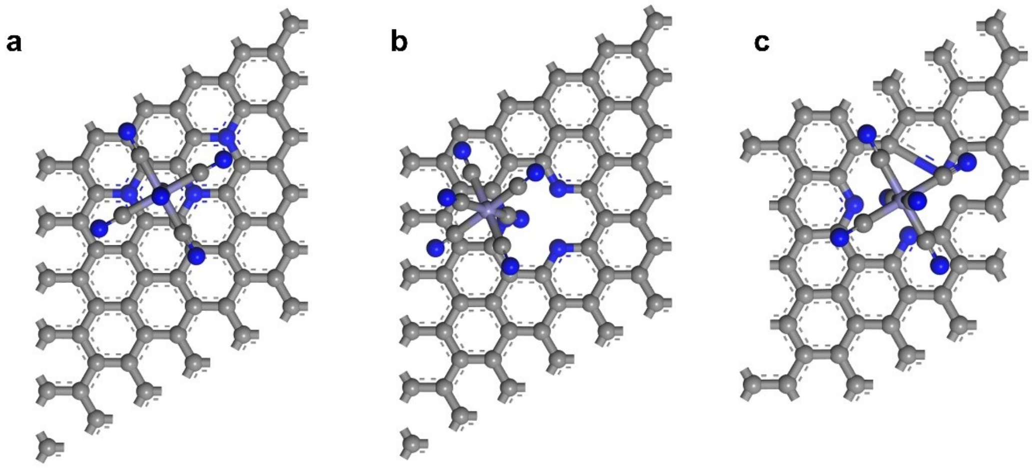

Fig. S11. Adsorbed structure of $Fe(CN)_6^{3-}$ and $Fe(CN)_6^{4-}$ on (a) graphitic-N, (b) pyridinic-N and (c) pyrrolic-N.

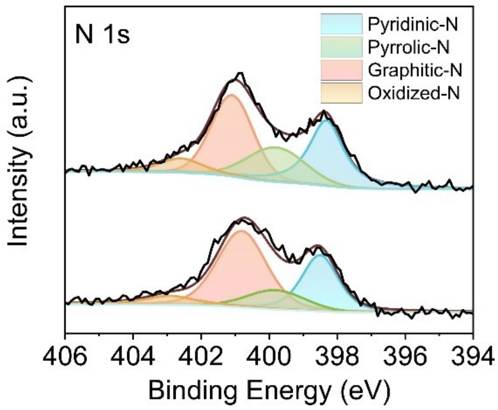

Fig. S12. N 1s XPS spectra of the N-CNW@CC before and after test in 0.4 M $K_3Fe(CN)_6/K_3Fe(CN)_6$ with peaks deconvoluted into pyridinic-N, pyrrolic-N, graphitic-N, and oxidized-N species respectively.

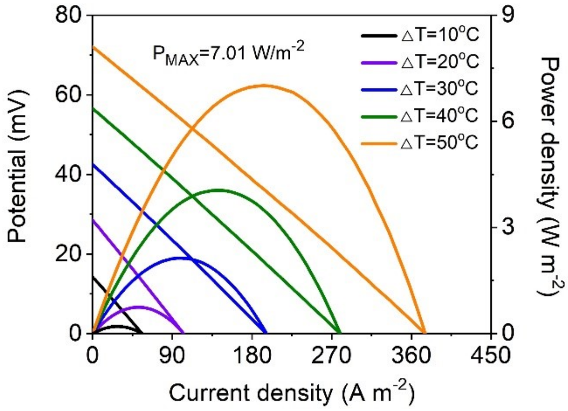

Fig. S13. Current-voltage curves and their corresponding power densities for N-CNW@CC-800 assemble in a modified TEC device with four-layer N-CNW@CC-800 electrodes for enhanced output.

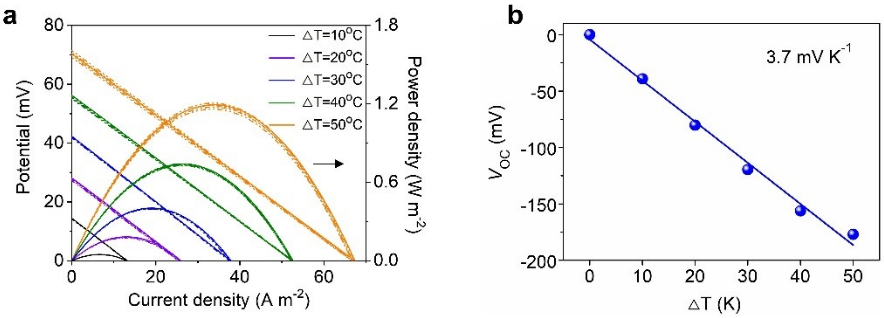

Fig. S14. (a) Current-voltage curves and their corresponding power densities for N-CNW@CC-800 assemble in a modified TEC device with four-layer N-CNW@CC-800 electrodes for enhanced output. (b) Open-circuit voltage (V_{oc}) of the TEC at different values of ΔT. The Seebeck coefficient (S_e) is calculated from the slope of the V_{oc}-ΔT curves.

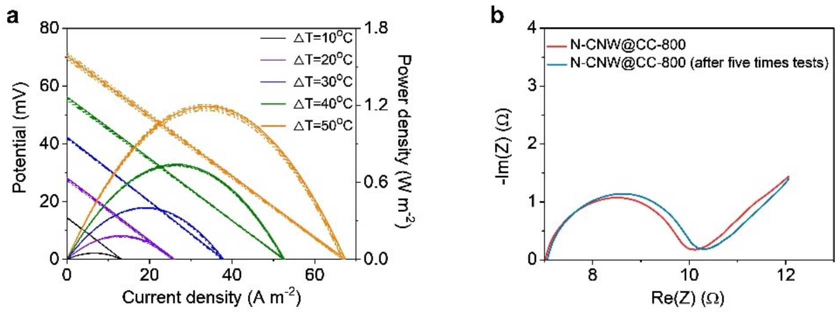

Fig. S15. (a) Current-voltage and their corresponding power densities curves of TEC assembled by N-CNW@CC-800, which were tested five times. (b) Nyquist impedance plots of N-CNW@CC-800 before and after five times tested.

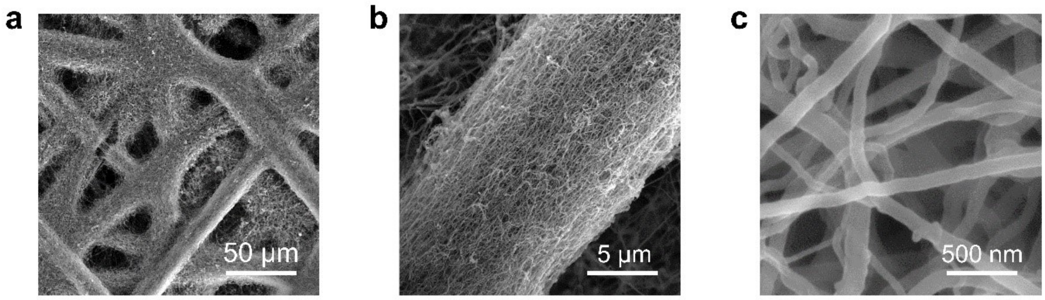

Fig. S16. SEM images of N-CNW@CP-800.

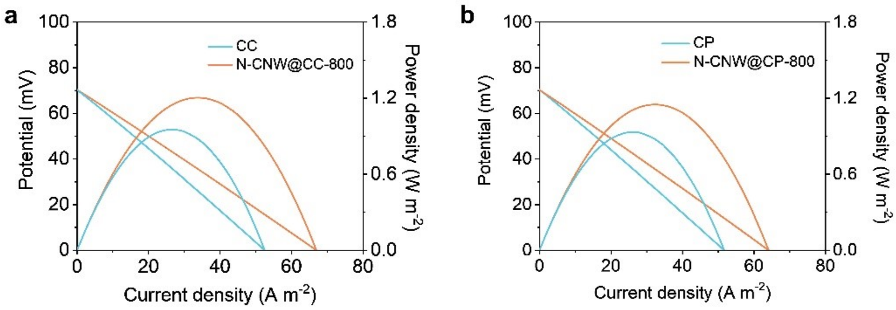

Fig. S17. Current-voltage and their corresponding power densities curves of TEC assembled by (a) carbon cloth and N-CNW@CC-800 and (b) carbon paper and N-CNW@CP. (ΔT=50^{o}C).

Table S1. Comparison of the thermoelectric property of TECs using N-CNW@CC electrode and optimized thermosensitive crystallization-boosted electrolyte (this work) with other electrolyte and electrode optimization reported in literatures.

Electrode	Electrolyte (ferro/ferricyanide redox couple)	ΔT (^oC)	P_{max} ($W\ m^{-2}$)	η_r (%)	Reference
N-CNW@CC	optimized thermosensitive crystallization-boosted aqueous electrolyte	40	17.45	13.02	This work
Carbon Paper	thermosensitive crystallization-boosted aqueous electrolyte	40	14.8	11.1	1
Anisotropic holey graphene aerogel	eutectic electrolyte consisting of formamide and water	106	3.6	0.7	2
Graphene-carbon sphere polylithic aerogels	water	~62	1.05	1.4	3
SWCNTs	water	20	0.09	0.275	4
SWNT-rGO composites	water	31	0.327	0.64	5
Activated carbon textile coated with carbon nanotubes	water	3.4	0.46	Not mentioned	6
Carbon mutli-walled nanotube foam	water	86	1.2	0.4	7
carbon nanotube aerogel sheet	water	51	6.6	3.95	8

Table S2. The ion diffusion coefficients from the EIS.

Sample	diffusion coefficients (σ)
Pure carbon cloth	0.114
N-CNW@CC (5 min)	0.098
N-CNW@CC (10 min)	0.095
N-CNW@CC (20 min)	0.092
N-CNW@CC (30 min)	0.095
N-CNW@CC(1 h)	0.094

1 B. Yu, J. Duan, H. Cong, W. Xie, R. Liu, X. Zhuang, H. Wang, B. Qi, M. Xu, L. Wang Zhong and J. Zhou, *Science*, 2020, **370**, 342-346.

2 G. Li, D. Dong, G. Hong, L. Yan, X. Zhang and W. Song, *Adv. Mater.*, 2019, **31**, 1901403.

3 D. Dong, H. Guo, G. Li, L. Yan, X. Zhang and W. Song, *Nano Energy*, 2017, **39**, 470-477.

4 T. J. Kang, S. Fang, M. E. Kozlov, C. S. Haines, N. Li, Y. H. Kim, Y. Chen and R. H. Baughman, *Adv. Funct. Mater.*, 2012, **22**, 477-489.

5 M. S. Romano, N. Li, D. Antiohos, J. M. Razal, A. Nattestad, S. Beirne, S. Fang, Y. Chen, R. Jalili, G. G. Wallace, R. Baughman and J. Chen, *Adv. Mater.*, 2013, **25**, 6602-6606.

6 H. Im, H. G. Moon, J. S. Lee, I. Y. Chung, T. J. Kang and Y. H. Kim, *Nano Res.*, 2014, **7**, 443-452.

7 L. Zhang, T. Kim, N. Li, T. J. Kang, J. Chen, J. M. Pringle, M. Zhang, A. H. Kazim, S. Fang, C. Haines, D. Al-Masri, B. A. Cola, J. M. Razal, J. Di, S. Beirne, D. R. Macfarlane, A. Gonzalez-Martin, S. Mathew, Y. H. Kim, G. Wallace and R. H. Baughman, *Adv. Mater.*, 2017, **29**, 1605652.

8 H. Im, T. Kim, H. Song, J. Choi, J. S. Park, R. Ovalle-Robles, H. D. Yang, K. D. Kihm, R. H. Baughman, H. H. Lee, T. J. Kang and Y. H. Kim, *Nat. Commun.*, 2016, **7**, 10600.